ISSN 1063-7842, Technical Physics, 2019, Vol. 64, No. 11, pp. 1657–1665. © Pleiades Publishing, Ltd., 2019.
Russian Text © The Author(s), 2019, published in Zhurnal Tekhnicheskoi Fiziki, 2019, Vol. 89, No. 11, pp. 1747–1755.

Columnar Niobium Oxide Nanostructures: Mechanism of Formation, Microstructure, and Electrophysical Properties

G. G. Gorokh[a],*, A. N. Pligovka[a], and A. A. Lozovenko[a]

[a] *Belarusian State University of Informatics and Radioelectronics, Minsk, 220113 Belarus*

**e-mail: gorokh@bsuir.by*

Received March 28, 2019; revised March 28, 2019; accepted April 15, 2019

Abstract—The morphology and microstructure of columnar niobium oxide nanostructures are studied and the dependences of their morphological sizes on anodizing voltages (100–450 V) and anodic alumina pore diameters (40–150 nm) are established. The features of ion transport during local anodization of niobium are studied and the transport numbers of electrolyte anions and niobium cations are calculated; a mechanism of formation and growth is proposed and the phase composition and electrophysical properties of columnar nanostructures are studied.

DOI: 10.1134/S1063784219110124

INTRODUCTION

The formation method of low-dimensional structures by anodizing layers of valve metals (Ti, Ta, Nb, Hf, Zr, W) through anodic alumina (AA) pores has been known for quite some time [1–3] but has developed intensively in recent years due to the prospects for the use of such nanostructure systems in new elements of micro-, nano- and optoelectronics [4–8]. By manufacturing an AA mask of preset sizes and selecting special conditions and regimes, it is possible to produce metal oxide nanostructures of a specific shape (protrusions, columns, columns with a modulated diameter [9], etc.) and with different oxidation states of the metal. Moreover, initially low-dimensional oxide formations of a valve metal are formed directly beneath pores but under certain conditions, they can fill pores partially or completely. It should be noted that the functional properties of nanostructures are primarily determined by their composition, as well as by the conditions of electrochemical and heat treatment. The oxides of each of these metals have their own specific properties, but among them niobium oxide stands out due to its unique electrophysical properties. Niobium compounds with oxygen having the oxidation states of +4, +3, and +2 are extremely unstable and the atoms tend to give away electrons and niobium in its highest oxidation state can be a part of anions and a part of cations [10, 11]. The character of chemical bond changes is conveniently traceable at the stages of gradual niobium oxidation. With the increase in valency, the basic character of niobium compounds is weakened, and the stability of compounds and the tendency to form coordination compounds increases. Oxides NbO and Nb_2O are typical metal compounds, NbO has metal conductivity, NbO_2 is a semiconductor, and Nb_2O_5 is a non-metallic oxide and has no electrical conductivity. Therefore, with an increase in the positive oxidation state, the fraction of metal bonds decreases and the fraction of covalent bonds increases. The half-occupied *d* orbitals are actively involved in the formation of chemical bonds of both a metal crystal and non-metallic compounds and their complexes [10, 12, 13]. In electrochemically formed nanostructures, all the above forms of niobium oxides are present simultaneously and, as expected, depending on the electrochemical treatment, their oxidation state may be different, therefore, their properties will be different. Therefore, by establishing a correlation between the conditions of formation, composition, and structure of niobium metal oxide nanostructures, it will be possible to predictably control their properties during their preparation.

This study presents the results of studying the morphological and structural characteristics of columnar niobium oxide nanostructures (CNONS) prepared by anodizing the thin-film bimetallic Al/Nb system in different acid electrolytes and reanodized at various voltages, describes the mechanism of their formation, and gives the results of their electrophysical studies.

1. SAMPLE PREPARATION AND MEASUREMENT TECHNIQUES

Silicon substrates, onto which 200 nm of Nb (bottom) and 1.5 μm of Al were deposited by vacuum magnetron sputtering, were used as initial samples. Electrochemical anodization of all experimental samples

was carried out in a potentiostatic mode in accordance with typical kinetics [6] at a temperature of 291 ± 0.5 K in the following electrolytes at voltages: in a 0.4M aqueous solution of $C_2H_2O_4$ at 37 V; in a 0.4 M aqueous solution of H_3PO_4 at 150 V; in a 0.2 M aqueous solution of $C_4H_6O_6$ at 250 V; and in a 0.2 M aqueous solution of $C_6H_8O_7$ at 300 V. The repeated high-voltage anodization (reanodization) of the niobium sublayer through AA pores formed under the above conditions was carried out in a 0.2 M aqueous solution of $C_6H_8O_7$ at voltages of 100, 150, 200, 250, and 300 V and in a 0.5 M aqueous solution of H_3BO_3 at 450 V. The electrical anodizing modes were set using a Keysight N5752A system DC power supply and recording and monitoring of in situ process parameters were carried out using a Keysight 34470A digital multimeter connected via a USB interface to a personal computer with Bench Vue software. After reanodization, the AA mask was removed in a 50% aqueous solution of H_3PO_4 at a temperature of 323 K.

The features of the nucleation and growth of CNONS in AA matrices were studied using scanning electron microscopy (SEM) on a Hitachi S-806 at an accelerating voltage of 20 kV and a Hitachi S4-800 at an accelerating voltage of 15 kV. The composition of the anodic niobium oxide (ANO) was studied by infrared spectroscopy, which is widely used for the analysis of thin films [14] including ANO [15]. The reflection spectra were recorded on an NEXUS E.S.P. IR Fourier spectrometer (Thermo Scientific, the United States) in the range of 2000–400 cm^{-1} and the spectral width of the gap of no more than 1 cm^{-1} in the reflection and multiple disturbed total internal reflection modes. Immediately prior to spectra recording, the samples were heated in a thermostat at 393 K for desorption of the condensed moisture from their surface. Purging of a spectrophotometer cell with dry air excluded the distortion of the spectra due to the absorption by atmospheric moisture.

The Auger profiles were recorded on an electron spectrometer equipped with an electron analyzer of the cylindrical mirror type [16]. The energy of the probing electron beam was 3 keV and the modulation voltage was 5 V. The intensity of Auger peaks dN/dE for the corresponding chemical elements (aluminum, niobium, silicon, and oxygen) was measured at a modulating voltage of 2.5 V in the energy range of 30–600 eV, recording the following characteristic Auger lines: 51 eV, the LMM transition in oxidized aluminum; 68 eV, the LMM transition in metallic (non-oxidized) aluminum; 203 eV, the KLL transition in niobium; and 510 eV, the KLL transition in oxygen [17]. Profiling was carried out by ion etching of the AA film with an Ar^+ ion beam with an energy of 2 keV.

The CNONS phase composition and microstructure were determined based on analysis of diffraction data obtained on a DRON-3 facility in CuK_α radiation at room temperature at a shooting rate of 60°C/h using the ICSD-PDF2 database (Release 2000), and POWDERCELL and FULLPROF programs.

The current–voltage characteristics were measured using a specialized probe device attached to the upper aluminum contact and to the substrate. The electric modes were set with a stepwise increase in voltage from 20 to 125 V using a Source Keysight 34401, the current–voltage characteristics were recorded using a Keysight B2901A parametric analyzer, and the measurement process was controlled using a USB interface in the EasyEXPERT group+ software environment. The measurements were carried out at temperatures in the range from 293 to 353 K.

2. RESULTS AND DISCUSSION

2.1. Study of the Morphology of Columnar Nanostructures

Figures 1a–1d show SEM images of niobium nanostructures formed in electrolytes of different nature at aluminum anodizing voltages after the AA matrix has been removed. The analysis of the images showed that the nature of the electrolyte and the electrical modes of the anodic polarization affect the nucleation process, shape, and size of the formed CNONS. It is noted that a feature of niobium nanostructures in the initial period of their growth is their goblet shape. The leg of a goblet is formed of bent and curved ropes, which, joining and filling the lower part of the pore, form a bowl. The height of the leg corresponds to the thickness of the barrier AA oxide layer (BOL), and the diameter of the bowl exceeds the pore diameter by a third. Presumably, the number of branches in the leg of such a goblet corresponds to the coordination number in the pore, i.e., the number of neighboring (adjacent pores) in AA. During anodizing when the barrier AA layer reaches niobium, its local oxidation begins due to the counter migration of Nb^{5+}, Al^{3+} cations, and O^{2-} anions along the path: substrate–BOL–electrolyte–electrode and back. Moreover, due to specific properties of niobium, its local oxidation does not begin only at the base of a hemispherical oxide AA cell, but also at the junction of cells at several points, forming thereby up to seven nanochannels in the barrier layer, through which due to their high ductility and fluidity under the action of the electric field, as well as due to volumetric growth as a result of the addition of oxygen, gradually oxidized niobium penetrates the pore base and merges into one columnar niobium oxide nanostructure.

The growth of CNONS continues due to the mutual migration of niobium and oxygen ions through the conducting niobium oxide, which contributes to the increase in nanochannel diameters in BOL and their merging. During the increase in the voltage of niobium anodizing and oxidation, there occurs the gradual final oxidation of aluminum regions under the

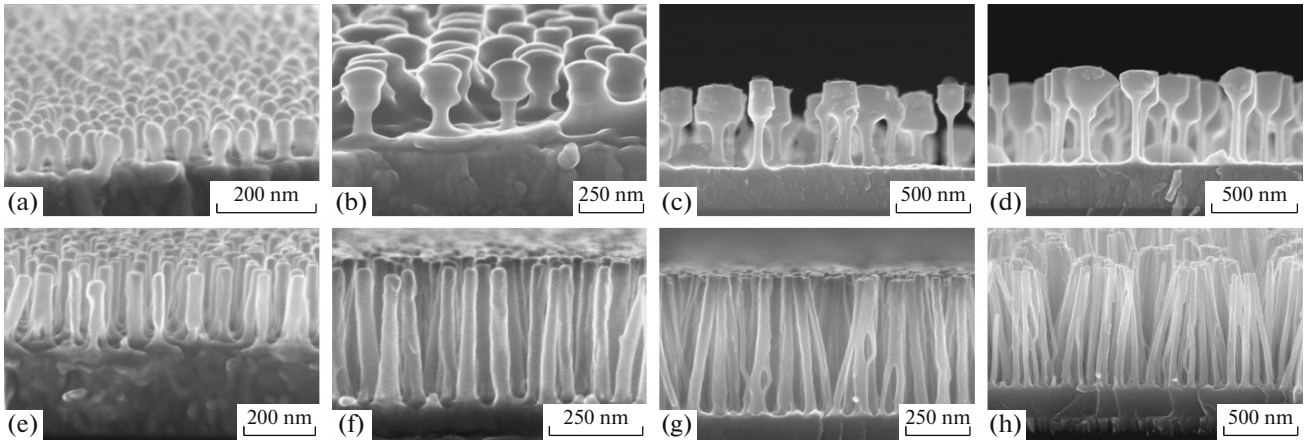

Fig. 1. Electron microscopy images of the cross sections of CNONS formed in: (a) a 0.4 M solution of oxalic acid at a voltage of 37 V; (b) a 0.4 M phosphoric acid solution at a voltage of 150 V; (c) a 0.2 M tartaric acid solution at a voltage of 250 V; (d) a 0.2 M solution of citric acid at a voltage of 300 V; as well as CNONS formed in a 0.4 M solution of oxalic acid at a voltage of 37 V and reanodized at a voltage of: (e) 100, (f) 200, (g) 300, and (h) 450 V.

pores. The diameters of the niobium columns become larger than the original pores in AA, which can be explained by the phenomenon of substitution during the growth of niobium columns, the same as in the case of tantalum [18]. The growth of columns along the AA pores competes with the extension of the bases of the columns, the distance between which decreases until they merge into the continuous oxide layer. The relationships between these competing phenomena affecting the development of the upper and lower parts of the film are determined by the coefficient of the volume growth, transport numbers of different niobium oxidation states, which can be complex values, and the ratio of ionic resistances of ANO and AA surrounding the columns. A deeper understanding of the mechanism of the growth and formation of niobium oxide nanostructures through the AA matrix was given by the calculation of the transport numbers of ANO columns formed in a 0.4 M solution of oxalic acid at a voltage of 37 V and reanodized at voltages of 100, 200, 300, and 450 V, images of which are shown in Fig. 1. The morphological parameters of these nanostructures, as measured by micrographs, are shown in Table 1.

The transport numbers for CNONS were determined at the following statements [18]: (1) the anodizing electrolytes do not dissolve either AA or CNONS; (2) electrolyte components are absent in CNONS; and (3) during reanodization, the increase in ANO leads to pore filling, and at the base of the pores, to the formation of a continuous ANO layer under porous AA. Thus, the interface between the upper and lower parts of the film can be used as a mark separating oxides formed due to the migration of cations and anions. Assuming that the niobium and oxide transfer coefficients are unchanged in the upper (oxide columns) and the lower (continuous ANO layer) parts of the film, the transport number of oxygen ions, t_O, can be calculated as:

$$t_O = \frac{V_{low}}{V_{tot}} = \frac{V_{low}}{V_{low} + V_{up}} = \frac{h}{(h + Nl\pi r^2)}, \quad (1)$$

where V_{low} is the specific volume per unit area of a continuous ANO layer formed under the AA pores, i.e., below the mark (bottom of the film); V_{up} is the specific volume per unit area of columnar ANO formed in the AA pores, i.e., above the mark (the upper part of the film); V_{tot} is the entire volume formed

Table 1

Voltage, V	h, nm	N, nm^{-2}	l, nm	r, nm	t_O	t_N
37	20	1.39×10^{-4}	80	21	0.56	0.44
100	40	1.4×10^{-4}	191	21.5	0.50	0.5
200	65	1.38×10^{-4}	348	20.8	0.49	0.51
250	91	1.35×10^{-4}	440	20.5	0.52	0.48
300	110	1.42×10^{-4}	548	21.4	0.5	0.5
450	185	1.4×10^{-4}	750	21	0.56	0.44

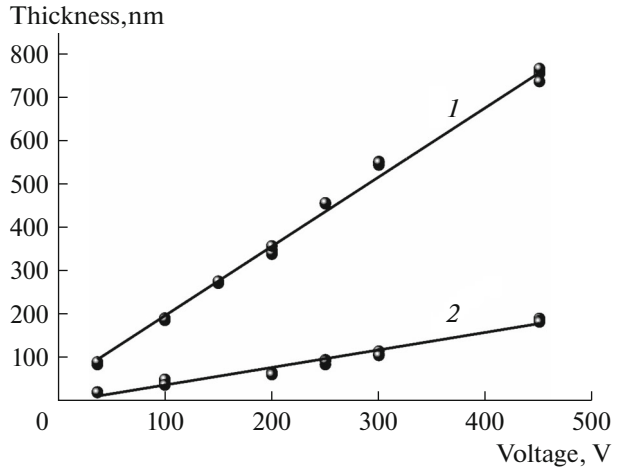

Fig. 2. Dependences of changes in the thickness of the upper columnar layer (*1*) and the lower continuous anodic niobium oxide layer (*2*) on the reanodization voltage of niobium through the AA pores.

by ANO per unit area (the lower and upper parts of the film); h is the thickness of the lower part of the film; N is the amount oxide columns per unit area; l is the height of oxide columns; and r is the radius of the oxide columns.

On the basis of the results given in Table 1, it is possible to conclude that the transport numbers of oxygen t_O and niobium t_N are independent of the anodizing voltage and are 0.5 for oxygen and niobium. Some deviation from 0.5 in one direction or another can be associated with the measurement error and the degree of the reproducibility of the conditions for the formation of nanostructures. The specific number of columns, pore diameters, and radii of the columns are independent of the reanodization voltage, and are determined by the formation voltage, which was 37 V. The column height and thickness of the lower continuous oxide layer increase in proportion to the increase on the reanodization voltage (Fig. 2).

2.2. Study of the Structure and Composition of Metal Oxide Columnar Films

Auger electron spectroscopy was used to study the oxygen content in CNONS and its ratio to niobium in columns from the top to the base. Figure 3 shows the distribution profile of Nb and O in CNONS formed in a 0.4 M oxalic acid solution at the voltage of 37 V and reanodized at 450 V. It can be seen from the profile that at the CNONS tops, O and Nb concentrations are 6.7 and 0.7 out of 9 rel. units, respectively (the silicon concentration can be ignored). As the middle of the column is approached, the oxygen concentration in the structures decreases, and the O and Nb concentrations are roughly the same near the continuous oxide layer. In the continuous layer under columnar structures, the niobium concentration increases and that of oxygen decreases accordingly, until the film passes into metallic niobium [19]. The relative niobium concentration in the continuous layer reaches 5.2 and that of oxygen is 1.2 that approximately corresponds to the ratio of 1 to 0.23 [19].

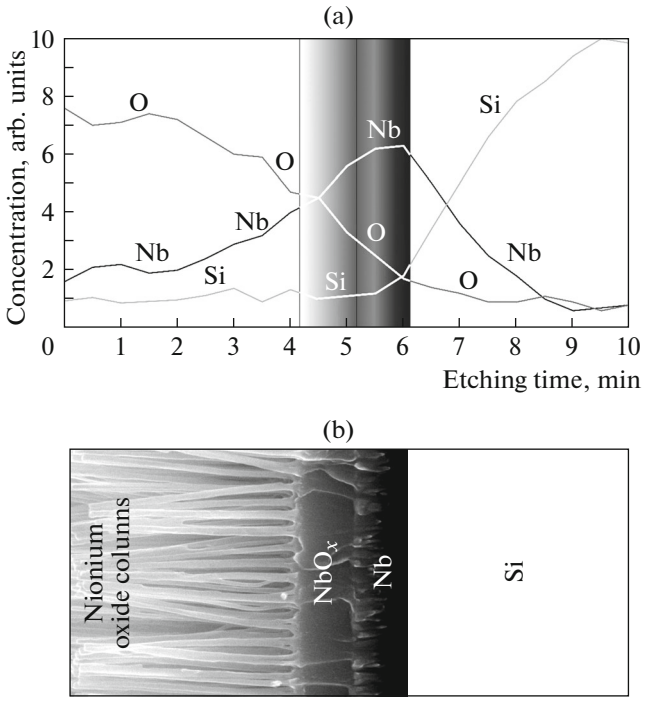

Fig. 3. Auger profile of CNONS formed at a voltage of 37 V and reanodized at 450 V (a); image of the studied structure (b).

In CNONS formed in a tartaric acid electrolyte at 250 V, the ratio of niobium and oxygen is somewhat different. The niobium concentration from the surface to the base increases from 60 to 80%, while the oxygen concentration varies from 20 to 15%, and the presence of silicon from the substrate is already noticeable in the lower part. After reanodization at 450 V, the ratio of elements changes dramatically: the niobium concentration increases from 20 to 50%, the oxygen concentration decreases from 70 to 20%, and silicon is present over the entire length of the column within 10% (Fig. 4).

The types of oxides that make up CNONS are determined by IR spectroscopy (Fig. 5). The character of the absorption bands of the film oxide (upper curve), which significantly differs from the pronounced and narrow bands of the columnar oxide (lower curve) characteristic for the ordered crystalline structure, indicates a predominantly amorphous structure of the oxide under the columns. As a result of the analysis of the spectra and the attribution of the absorption bands in the spectra of experimental samples, it can be assumed that CNONS formed in a solution of oxalic acid consist of at least three oxide phases

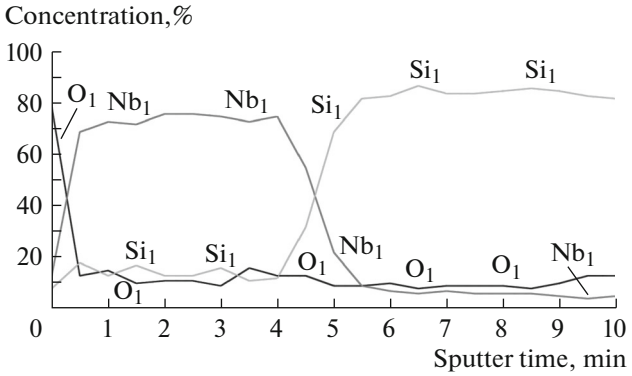

Fig. 4. Auger profile of CNONS formed in a 0.2 M solution of tartaric acid at a voltage of 250 V and reanodized at 450 V.

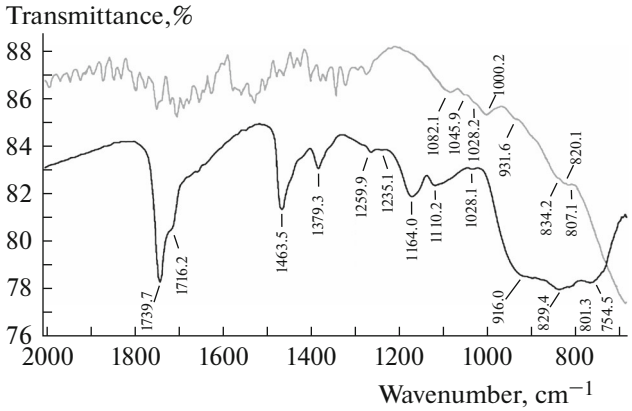

Fig. 5. Infrared absorption spectra of CNONS formed in a 0.2 M solution of oxalic acid at a voltage of 37 V.

in the Nb–O system out of the five known: NbO, NbO_2, and Nb_2O_5, mainly with reduced oxygen content (NbO), while Nb_2O_5 is present in two known modifications: α-Nb_2O_5 and β-Nb_2O_5 [21]. Moreover, in the oxide formed at 37 V, the intensity of the absorption bands corresponding to the lower forms of oxides is much higher. The increase in the formation voltage during the reanodization up to 450 V leads to an increase in the amount of Nb_2O_5 as indicated by the increase in the intensity of the absorption band with $\nu_{max} = 1110$ cm^{-1} [22]. The observed increase in the absorption (in comparison with other bands) at wavenumbers of 829 and 801 cm^{-1}, gradually overlapping and turning into a wide absorption band at approximately 916–754 cm^{-1}. The content of NbO_2 in the composition of CNONS varies slightly, however, the localization of the absorption band at $\nu_{max} = 1164$ cm^{-1} in reanodized samples may indicate the increase in more ordered dioxide in the composition of oxide columns. Moreover, the amount of amorphous pentoxide also increases [23]. It can be assumed that the increase in the formation voltage of the columnar oxide leads to the formation of a noticeable amount of trivalent niobium oxide in its composition. In addition, the content of Nb oxide, which has an absorption at approximately 1128 cm^{-1}, increases (it is possible that the band intensity increases due to the crystallization of Nb_2O_5).

The microstructure, elemental, and phase composition of CNONS were studied by X-ray analysis. Figure 6 shows the X-ray diffraction patterns of the CNONS samples formed in a 0.2 M solution of oxalic acid at 37 V and reanodized at 100 and 300 V, and annealed at 400°C (Figs. 6a, 6b) and 800°C (Figs. 6c, 6d). It was found that most of the oxide phases for the images annealed at 400°C have a monoclinic crystal lattice. Most oxide phases are characterized by a quantitative increase with increasing anodizing voltage, which is explained by the increase in the volume of the oxidized niobium metal film and field overstrength in the columnar nanostructure, which leads to the oxygen redistribution and the formation of additional oxide phases [24]. However, there are differences, peaks at 34.6° and 41.7° correspond to the NbO_2 and Nb_2O_5 oxide phases and are not identified in 100 V samples and differ in the maximum integrated intensity in 300 V samples. This feature may be related to oxygen redistribution, which leads to the decay of one phase and the formation of another one due to the increase in the anodization voltage [25]. In this case, it can be assumed that for samples with a voltage of 100 V, the volume of oxide phases is generally small, and the three largest peaks at 2Θ angles, 38.6° and 82°, are responsible for silicon and metallic niobium.

Figures 6c and 6d shows the diffraction patterns for samples formed at voltages of 100 and 300 V and annealed in vacuum at temperature of 800°C. The following features are characteristic of these diffraction patterns. The peaks (37.44°, 69.38°, and 82.28°) characteristic of metallic niobium disappear in the spectra. This feature can be explained by the fact that, at temperatures above 600°C, oxide groups begin to decompose and all oxygen located in the boundary oxide layer begins to penetrate into the metallic niobium film and oxidize it with the formation of the NbO oxide phase [26, 27]. This process continues until the metal film is completely oxidized. Metallic niobium in CNONS at a temperature of 550–600°C is still present; thermal heating leads to the thermal oxidation of niobium and the integrated peak intensity characteristic of metallic niobium at a temperature of 400°C decreases and completely disappears at 800°C. In this case, new modifications of the Nb_2O_5 oxide phases with peaks at 22.7°, 28.4°, 36.8°, and 54.2°, as well as NbO_2 with a peak at 43.8°, appear.

All samples are characterized by the appearance of niobium disilicide at a temperature of vacuum annealing above 800°C. This can be explained by the formation of $NbSi_2$ on the silicon substrate/niobium inter-

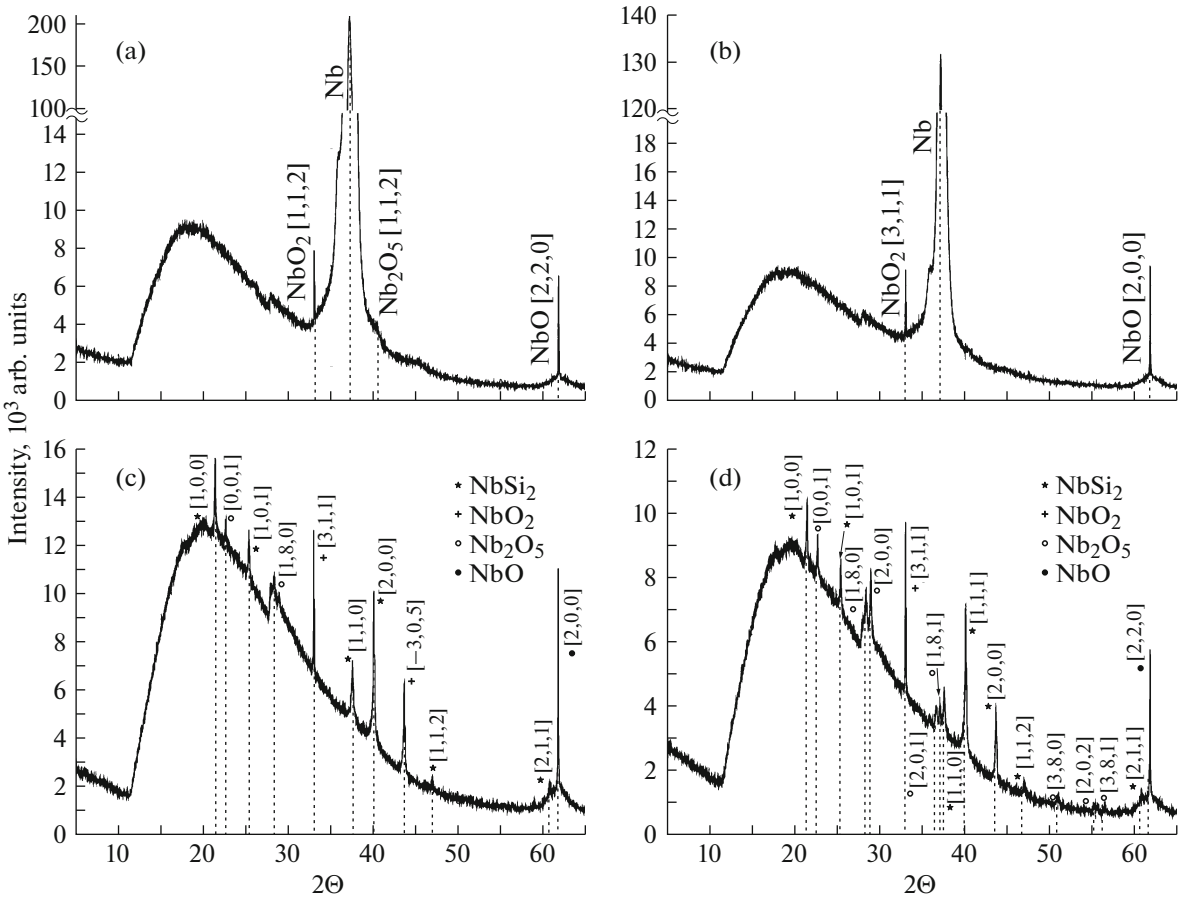

Fig. 6. X-ray diffraction patterns of CNONS formed in a 0.2 M solution of oxalic acid at a voltage of 37 V and reanodized at 100 V (a, c) and 300 V (b, d), and annealed at 400°C (a, b) and at 800°C (c, d).

face under the effect of high temperature [20] and the specific properties of niobium (good adhesion of niobium to silicon, the presence of free oxygen, high mobility, etc.).

The analysis of the elemental and phase compositions of niobium oxide nanostubes consisting of a mixture of the α-Nb(O) solid solution with a bcc lattice and three stable oxide modifications: NbO, NbO_2, and Nb_2O_5, with the predominant content of the last phase at the top of the columns, as well as the character of its modification from peaks to the base, makes it possible to predict and produce the growth centers of arrays of metal oxide nanostructures pre-distributed in a predetermined manner. The data obtained make it possible to establish a correlation between the formation conditions, structure, and properties of nanostructured ANO, and can be used to model the output characteristics of a nanostructured material based on nanotubes of niobium oxide. Data on the crystal structure of niobium columns are important in terms of electrical conductivity and the stability of their electrophysical properties over time.

2.3. Study of the Electrophysical Characteristics of CNONS

The electrophysical characteristics of CNONS were studied on samples formed in a 0.2 M solution of oxalic acid at 37 V and reanodized at 300 and 450 V. After that, the prepared structures were subjected to chemical etching in a solution based on a mixture of chromic and phosphoric acids (the so-called "selective etchant" [2]) at a temperature of 323 K for 12 min. As a result of this procedure, a part of the AA matrix, the pores of which were not filled with ANO, was removed from the samples, and at the same time, the tops of the columns became bare (Figs. 7a, 7b). The average diameters of CNONS were ~40 nm. The thickness of the columnar layer was about 800 nm. The thickness of the continuous niobium metal oxide layer did not exceed 225 nm and the non-oxidized niobium layer was ~200 nm. The columns protruded from the AA surface at about 40 nm. Aluminum contacts were formed on surface samples 1 μm thick and 1 × 1 mm in area. The obtained structure is schematically shown in Fig. 7c.

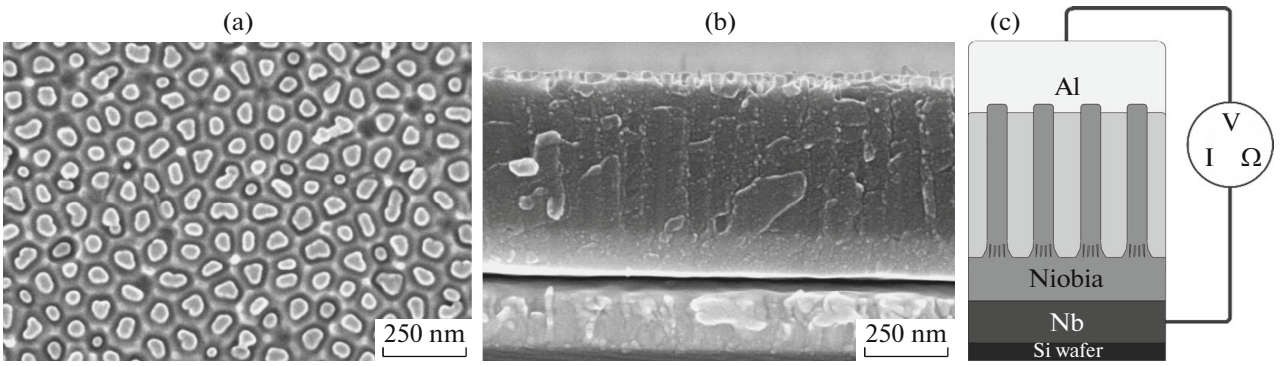

Fig. 7. Electron microscopy images of the surface (a) and cross section (b) of the structure with CNONS in the AA matrix; schematic image of the structure for measuring the CVC (c).

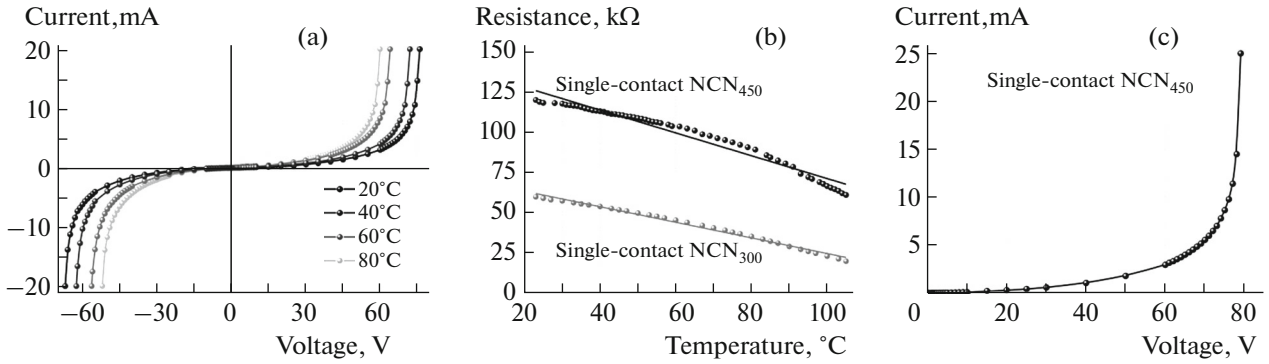

Fig. 8. CVC of CNONS in the AA matrix (a); temperature dependences of the electrical resistance of CNONS formed at 300 and 450 V (b); CVC of CNONS formed at 450 V measured with increasing voltage from 0 V to the voltage breakdown (c).

Figure 8a shows the I–V characteristics when the current passed through arrays of niobium nanocolumns in AA pores between the contacts on niobium at the base of the columns and on their surface on aluminum at various temperatures. The I–V characteristics of the CNONS arrays had an exponential dependence of the current on the changing voltages during direct and reverse switching. The currents through nanowires reached 2 mA at 20 V and a temperature of 20°C and increased to 62 mA with increasing temperature to 80°C. The increase in the temperature led to a decrease in control voltages from 75 to 45–50 V upon reaching a tripping current (65 mA). The observed nonlinearity of the I–V characteristics and their temperature dependences can be related, as we assume, to the presence of the metal–semiconductor on the upper aluminum contact [28], transport properties of the columns themselves, which are diffuse and consist of oxides with different types of the conductivity, as well as the presence of a contact transition of a continuous niobium oxide layer and metallic niobium. It should be borne in mind that the NbO_2/Nb transition is not sharp but has a certain thickness. At the reverse switching of the structure, the shape of the I–V characteristic differs little from that of direct switching, here the valve properties of niobium oxide at the interface with the metal, which has different electrical conductivities in direct and reverse switching, are manifested. At reverse switching, control voltages at maximum currents are about 5 V lower than those at direct switching. Thus, the character of the current dependence is determined by both the contact phenomena at the upper and lower contacts and the heterogeneity of the distribution of charge carriers in the columns themselves [29].

The temperature dependences presented in Fig. 8b show a linear decrease in the resistance with increasing temperature in the measured system with CNONS formed at 300 and 450 V. The shape of the resistance dependence in the measured system is likely to be affected by both the upper metal–semiconductor contact and the lower Nb/NbO_2 contact. The resistance of columnar arrays in the AA matrices formed at 300 V at room temperature was about 60 kΩ, while that for CNONS reanodized at 450 V exceeded ~125 kΩ. Upon heating to 80°C, the resistance of the first structures decreased to 20 kΩ, while that of the CNONS formed at 450 V decreased to 65 kΩ. Thus, the relative decrease in the resistivity is significantly higher in the structures obtained by reanodization at 300 V. The

calculated temperature coefficient of the electrical resistance is negative, and its value is: -1.39×10^{-2} K^{-1} and -1.28×10^{-2} K^{-1} for structures formed at voltages of 300 and 450 V, respectively.

If the phase composition in these two structures is compared, then the quantitative content of Nb_2O_5 in the columns formed at 450 V is much larger than that in structures obtained at 300 V, where the highly conductive NbO_2 oxide predominates. At strong heating, as well as at the impact of the high electric field as a result of self-heating, NbO_2 can be forced to give off its oxygen. With the loss of oxygen, NbO_2 passes into the lower NbO oxide, which perfectly conducts electric current. At long-term impact, all oxygen is also split off rather quickly, and the metallic type of the conductivity may be manifested in the structures. At the stepwise increase in the voltage without current limitation, breakdown occurs at 80 V at the plates of structures obtained at 450 V (Fig. 8c). When switched on again, the resistance does not exceed 2–6 Ω, which corresponds to a breakdown of a similar MDM structure [30].

CONCLUSIONS

The morphological and structural characteristics of CNONSs formed by reanodization at voltages of 100–450 V through AA matrices with pore sizes of 40–150 nm were studied. The dependences of the change in the microgeometric dimensions of columnar nanostructures on the reanodization voltage are established. A mechanism for the growth of CNONS is proposed and the transport numbers of niobium ions are determined during its anodization through AA pores. The analysis of the composition and microstructure of niobium columns and the effect of the conditions of formation and thermal annealing on them is carried out. Using Auger electron spectroscopy, it was found that in CNONS, the niobium concentration from the surface to the base increases from 60 to 80%, while the oxygen concentration varies from 20 to 15%. After reanodization, the niobium concentration increases from 20 to 50%, and oxygen decreases from 70 to 20%. Three oxide phases in the Nb–O system: NbO, NbO_2, and Nb_2O_5, with the predominant content of the last phase at the top of the columns, which is present in two modifications: α-Nb_2O_5 and β-Nb_2O_5, were determined by IR spectroscopy as part of CNONS. After reanodization, the amount of pentoxide and niobium dioxide increases. CNONS are a metal oxide semiconductor with an exponential CVC. The temperature coefficient of the electrical resistance of the columnar niobium oxide nanostructures is negative and is approximately -1.4×10^{-2} K^{-1}. The obtained data make it possible to determine the required thicknesses of all layers and the anodizing modes in order to reproducibly and controllably obtain arrays of ANO columns with the required microgeometry, structure, composition, and properties.

FUNDING

This work was supported by the State program for scientific research of the Republic of Belarus Convergence 2020 (task 3.3) and the scientific and technical program of the Union State Technology-SG (task 2.3.2.1).

CONFLICT OF INTEREST

The authors declare that they do not have any conflicts of interest.

REFERENCES

1. A. I. Vorobyova, V. A. Sokol, and E. A. Outkina, Appl. Phys. A **67**, 487 (1998). https://doi.org/10.1007/s003390050808
2. A. I. Vorobyova and E. A. Outkina, Thin Solid Films **324**, 1 (1998). https://doi.org/10.1016/s0040-6090(97)01194-2
3. V. F. Surganov, A. M. Mozalev, and A. A. Poznyak, Zh. Prikl. Khim. **68**, 1466 (1995).
4. V. F. Surganov and G. G. Gorokh, Proc. SPIE **4019**, 526 (2000). https://doi.org/10.1117/12.382321
5. A. Mozalev, M. Sakairi, I. Saeki, and H. Takahashi, Electrochim. Acta **48**, 3155 (2003). https://doi.org/10.1016/S0013-4686(03)00345-1
6. A. Mozalev, G. G. Gorokh, M. Sakairi, and H. Takahashi, J. Mater. Sci. **40**, 6399 (2005). https://doi.org/10.1007/s10853-005-1620-9
7. A. Mozalev, H. Habazaki, and J. Hubálek, Electrochim. Acta **82**, 90 (2012). https://doi.org/10.1016/j.electacta.2012.05.065
8. Z. Pytlicek, M. Bendova, J. Prasek, and A. Mozalev, Sens. Actuators, B **284**, 723 (2019). https://doi.org/10.1016/j.snb.2019.01.009
9. A. Pligovka, A. Zakhlebayeva, and A. Lozovenko, J. Phys.: Conf. Ser. **987**, 012006 (2018). https://doi.org/10.1088/1742-6596/987/1/012006
10. S. Albrecht, C. Cymorek, and J. Eckert, in *Ullmann's Encyclopedia of Industrial Chemistry* (Wiley, 2011), Vol. 24, p. 133. https://doi.org/10.1002/14356007.a17_251.pub2
11. R. A. Rani, A. S. Zoolfakar, A. P. O'Mullane, M. W. Austin, and K. Kalantar-Zadeh, J. Mater. Chem. A **2**, 15683 (2014). https://doi.org/10.1039/c4ta02561j
12. E. I. Ko and J. G. Weissman, Catal. Today **8**, 27 (1990). https://doi.org/10.1016/0920-5861(90)87005-n
13. C. Oki, G. Sajiki, S. Sakida, Y. Benino, and T. Nanba, J. Ceram. Soc. Jpn. **124**, 1221 (2016). https://doi.org/10.2109/jcersj2.16180
14. B. H. Stuart, *Infrared Spectroscopy, Fundamentals and Applications* (Wiley, 2004).
15. P. J. Larkin, *Infrared and Raman Spectroscopy: Principles and Spectral Interpretation* (Elsevier, 2011).
16. *Practical Surface Analysis by Auger and X-Ray Photoelectron Spectroscopy*, Ed. by D. Briggs and M. Seah (Wiley, New York, 1983).

17. L. E. Davis, N. C. MacDonald, P. W. Palmberg, and G. E. Riach, *Handbook of Auger Electron Spectroscopy* (Perkin-Elmer, Eden Prairie, 1978).
18. A. Mozalev, A. J. Smith, S. Borodin, A. Plihauka, A. W. Hassel, M. Sakairi, and H. Takahashi, Electrochim. Acta **54**, 935 (2009). https://doi.org/10.1016/j.electacta.2008.08.030
19. A. N. Pligovka and G. G. Gorokh, in *Nanostructures in Condensed Media* (Inst. Teplo- i Massoobmena, Minsk, 2014), p. 310.
20. M. Ukegawa, A. Yamauchi, A. Kobayashi, and K. Kurokawa, Vacuum **83**, 157 (2008). https://doi.org/10.1016/j.vacuum.2008.04.080
21. A. Fielicke, G. Meijer, and G. von Helden, J. Am. Chem. Soc. **125**, 3659 (2003). https://doi.org/10.1021/ja0288946
22. M. S. P. Francisco and Y. Gushikem, J. Mater. Chem. **12**, 2552 (2002). https://doi.org/10.1039/b200685e
23. J.-M. Jehng and I. E. Wachs, Chem. Mater. **3**, 100 (1991). https://doi.org/10.1021/cm00013a025
24. V. S. Braga, F. A. C. Garcia, J. A. Dias, and S. C. L. Dias, J. Therm. Anal. Calorim. **92**, 851 (2008). https://doi.org/10.1007/s10973-006-8325-4
25. A. Mozalev, R. M. Vázquez, C. Bittencourt, D. Cossement, F. Gispert-Guirado, E. Llobet, and H. Habazaki, J. Mater. Chem. C **2**, 4847 (2014). https://doi.org/10.1039/c4tc00349g
26. L. K. Frevel and H. W. Rlnn, Anal. Chem. **27**, 1329 (1955). https://doi.org/10.1021/ac60104a035
27. A. M. Raba, J. Bautista-Ruiz, and M. R. Joya, Mater. Res. **19**, 1381 (2016). https://doi.org/10.1590/1980-5373-mr-2015-0733
28. L. Yang, Z. Wang, D. Li, and Z. Zhang, Vacuum **140**, 165 (2017). https://doi.org/10.1016/j.vacuum.2017.01.015
29. A. Pligovka, A. Lazavenka, and A. Zakhlebayeva, *Proc. 18th IEEE Int. Conf. on Nanotechnology, Cork, Ireland, 2019*. https://doi.org/10.1109/NANO.2018.8626387
30. A. N. Pligovka, A. N. Luferov, R. F. Nosik, and A. M. Mozalev, *Proc. Int. Crimean Conf. Microwave and Telecommunication Technology, Sevastopol, Ukraine, 2010*, p. 880. https://doi.org/10.1109/CRMICO.2010.5632734

Translated by L. Mosina